

Classical estimates of the effective thermoelastic properties of copper–graphene composites^{*}

Przemysław Sadowski^{*}, Katarzyna Kowalczyk-Gajewska,
Stanisław Stupkiewicz

*Institute of Fundamental Technological Research (IPPT),
Pawińskiego 5B, 02–106 Warsaw, Poland*

Abstract

Significant research effort is concentrated worldwide on development of graphene-based metal-matrix composites with enhanced thermomechanical properties. In this work, we apply two classical micromechanical mean-field theories to estimate the effective thermoelastic properties that can be achieved in practice for a copper–graphene composite. In the modelling, graphene is treated as an anisotropic material, and the effect of its out-of-plane properties, which are less recognized than the in-plane properties, is studied in detail. To address the severe difficulties in processing of graphene-based metal-matrix composites, the copper–graphene composite is here assumed to additionally contain, due to imperfect processing, particles of graphite and voids. It is shown quantitatively that the related imperfections may significantly reduce the expected enhancement of the effective properties. The present predictions are also compared to the experimental data available in the literature.

Key words: A. Metal-matrix composites (MMCs); B. Mechanical properties; B. Thermal properties; C. Micro-mechanics; Graphene

1 Introduction

Exceptional properties of graphene make it a natural candidate for production of composite materials with enhanced thermomechanical properties. In fact,

^{*} Published in Composites Part B (2015), doi:10.1016/j.compositesb.2015.06.007

^{*} Corresponding author.

Email addresses: psad@ippt.pan.pl (Przemysław Sadowski),
kkowalcz@ippt.pan.pl (Katarzyna Kowalczyk-Gajewska),
sstupkie@ippt.pan.pl (Stanisław Stupkiewicz).

simple estimates, such as the rule of mixtures, show that properties of popular polymers and metals could be significantly improved even by a small addition of graphene. However, the results obtained in practice are often not so spectacular as one might expect. This may be due to difficulties in processing of graphene-based composites, structural defects in the final products and in the graphene itself, presence of contaminants and interactions between graphene and the matrix material.

The aim of the present study is to estimate the effective thermomechanical properties that can be achieved in practice for graphene-reinforced metal-matrix composites, and specifically for copper-graphene composites. In particular, we show quantitatively that the expected gain in the effective properties can be significantly reduced for an imperfectly processed copper-graphene composite that additionally contains particles of graphite and voids so that the composite is effectively a multiphase composite. We also study the influence of out-of-plane properties of graphene and show that they significantly affect the effective properties.

Pristine graphene (i.e., a single layer of hexagonally arranged carbon atoms) exhibits outstanding in-plane thermal and mechanical properties. The in-plane thermal conductivity reaching 5300 W/mK has been measured [1], and the in-plane Young's modulus of 1000 GPa is typically reported [2]. However, those values refer to idealized conditions of measurements for individual graphene platelets. Atomic defects [3], interfacial interactions with a substrate or matrix material [4–7], and increased number of carbon layers [3, 8, 9] may lead to significantly lower values measured in reality, c.f. [10]. In particular, it is distinguished between single-, double- and few- (between 3 and 10) layer graphene as three different types of 2D crystals [11] with different chemical, physical and mechanical properties.

Graphene-reinforced polymer-matrix composites are widely examined experimentally and theoretically, e.g. [10, 12–14]. The results indicate that polymer-graphene composites are promising multifunctional materials with significantly improved tensile strength, elastic modulus, and electrical and thermal conductivity. Note, however, that typical polymers are characterized by low elastic stiffness and low thermal conductivity so that the contrast of properties is very high and enhancement of thermomechanical properties is relatively easy upon successful addition of even a small amount of graphene.

A different situation is encountered in the case of metal-matrix composites, and here the progress is so far quite limited [8, 15–17]. The reasons are twofold. Firstly, metals are characterized by higher elastic stiffness and higher thermal conductivity, hence the contrast of properties is lower than in the case of polymer-matrix composites. Secondly, the technological difficulties in processing of graphene-reinforced metal-matrix composites are more pronounced than

in the case of polymer-matrix composites. The related difficulties include inhomogeneous distribution of graphene platelets (they tend to segregate from metal particles and form agglomerates due to van der Waals forces [18]), porosity caused by agglomeration of graphene platelets and insufficient densification of metal powders [19–21], relatively high processing temperature (over 1000°C in the case of copper) at which graphene is easily decomposed or damaged during traditional processes of powder metallurgy [18]. As a result, the potential benefits of graphene may be easily lost or strongly reduced [19].

Moreover, it is difficult to produce a composite reinforced solely by the pristine graphene. Depending on the processing technique, inclusions of graphene of varying thickness can be obtained in practice. As already discussed, the properties of graphene depend strongly on the number of layers [8, 9, 11, 22], and structures with more than approximately 10 layers are usually not treated as graphene [11, 22]. In particular, it is expected that, with increasing number of layers, the properties of the structure would evolve from those of graphene to those of graphite. To address this issue, in the present work we assume that a graphene-based composite may additionally contain particles of graphite that correspond to thicker graphene-like structures or to other carbon-based inclusions resulting from the processing of the composite. As the thermoelastic properties of those particles, we adopt the properties of either crystalline or polycrystalline graphite, and we study the influence of those particles on the effective properties of the related graphene-based composites.

Effective thermomechanical properties of graphene-based composites are controlled not only by its exceptionally high in-plane stiffness and thermal conductivity but also by the corresponding out-of-plane properties. Since graphene originates from graphite which is highly anisotropic [23], it is expected to be highly anisotropic as well. In particular, its out-of-plane properties are expected to be significantly lower than the corresponding in-plane properties, just like in the case of crystalline graphite. However, the out-of-plane properties of graphene are less recognized, and they are significantly influenced by interfacial interactions [4, 5, 18, 21, 24]. Considering the ambiguity concerning the out-of-plane properties of graphene, their impact on the effective properties of isotropic and anisotropic composites has been examined in the present work.

Clearly, the high in-plane properties of graphene could be optimally utilized if the graphene platelets were preferentially oriented along a specified direction thus leading to a macroscopically anisotropic composite. However, controlling the orientation of graphene platelets and adequate processing of a bulk composite material is difficult [8, 25, 26], particularly in the case of metal–matrix composites [18, 21, 27, 28]. This is more feasible in the case of graphene deposited on thin films [29].

Computational modelling of functional properties of graphene and simulation of graphene–substrate or graphene–matrix interactions is an active area of computational material science. Investigation of quantum and atomic-scale effects requires application of adequate techniques, such as quantum chemistry, molecular dynamics and Monte-Carlo method, see e.g. [24, 30–32]. However, those approaches typically concern highly idealized conditions, and they are computationally demanding. Hence, applicability of those approaches to predictive modelling of graphene-based composites is limited.

An alternative approach is to apply classical micromechanical mean-field theories which are well developed, see [33–37], and proved highly successful in predictive modelling of composite materials, as well as in multi-objective optimization of their microstructure [38, 39]. The corresponding micromechanical averaging schemes are relatively simple so that estimates of effective thermo-mechanical properties can be obtained without excessive computational effort at the cost that some nano-effects are neglected.

The approach mentioned above has been followed in several works concerned with graphene-based composites. Often, the simplest rule of mixtures is used [8, 21, 30, 40], which corresponds to the Voigt upper bound (or to the Reuss lower bound in the case of the inverse rule of mixtures). The Mori–Tanaka method [41] has been used in [26] to estimate the effective elastic properties of nano-composites with graphene sheets dispersed in polymer matrix. However, it has been assumed that the cross-plane elastic modulus of graphene is 100 times higher than the in-plane modulus [26]. This assumption has not been justified and seems non-physical. In [19], the Halpin–Tsai model [42] has been used to predict the effective Young’s modulus of a copper–graphene composite. The aspect ratio of the inclusions has been taken into account, while graphene has been modelled as an isotropic solid, i.e., its cross-plane modulus has been assumed to be equal to the in-plane modulus. The effective medium approach accounting for the interfacial thermal resistance [43] was used in [44, 45] to estimate the effective properties of graphene-based composites.

The present work is concerned with micromechanical modelling of graphene-based metal-matrix composites with the focus on copper–graphene composites. One of the main goals of producing such composites is to enhance their thermoelastic properties, mostly the thermal conductivity. Accordingly, our aim in this work is to study quantitatively the enhancement that can be achieved in practice, and several factors are considered that may influence the overall properties of a copper–graphene composite:

- (1) In view of the ambiguity concerning the out-of-plane properties of graphene, their impact on the effective properties is examined in detail.
- (2) It is assumed that the copper–graphene composite may additionally contain other types of inclusions as a result of imperfect processing. Specif-


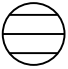

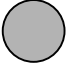

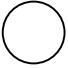
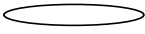
				Gn	graphene platelets
spherical crystalline graphite	SCGt			DCGt	disc-shaped crystalline graphite
spherical polycrystalline graphite	SGt			DGt	disc-shaped polycrystalline graphite
spherical voids	SV			DV	disc-shaped voids

Fig. 1. Types of inclusions considered in this work. The corresponding graphical symbols and abbreviations are used throughout the paper.

ically, we consider inclusions of crystalline and polycrystalline graphite and voids, all in either spherical or disc-like shape, see Fig. 1.

- (3) The types of two-, three- and four-phase composites studied in the paper are summarized in Figs. 2 and 3. Two general classes of composites are considered: macroscopically isotropic composites that correspond to random orientation of inclusions (Fig. 2) and transversely isotropic composites in which the disc-shaped inclusions are perfectly aligned (Fig. 3).

For all microstructures discussed above, the effective thermoelastic properties have been estimated using two classical mean-field models: the Mori–Tanaka (MT) model [41, 46] and the effective-medium-field (EMF) model [47].

The paper is organized as follows. The basic equations of the micromechanical theory used in the present study are summarized in Section 2. The specific assumptions adopted in the modelling and the material parameters characterizing the individual phases are provided in Section 3.1. Micromechanical predictions for macroscopically isotropic two-phase and multiphase composites are reported in Sections 3.2 and 3.3, respectively, while transversely isotropic composites are studied in Section 3.4. Finally, a comparison to available experimental data is presented in Section 3.5.

2 Effective thermoelastic properties of multiphase composites

In this section, we provide the formulation and the basic equations that can be applied to estimate the effective thermoelastic properties (elastic moduli, thermal expansion coefficient and thermal conductivity) of a multiphase composite. The focus is on materials composed of two or more types of inclusions embedded in a matrix, where the type of an inclusion is specified by its properties and shape. The adopted micromechanical modelling approach is based on

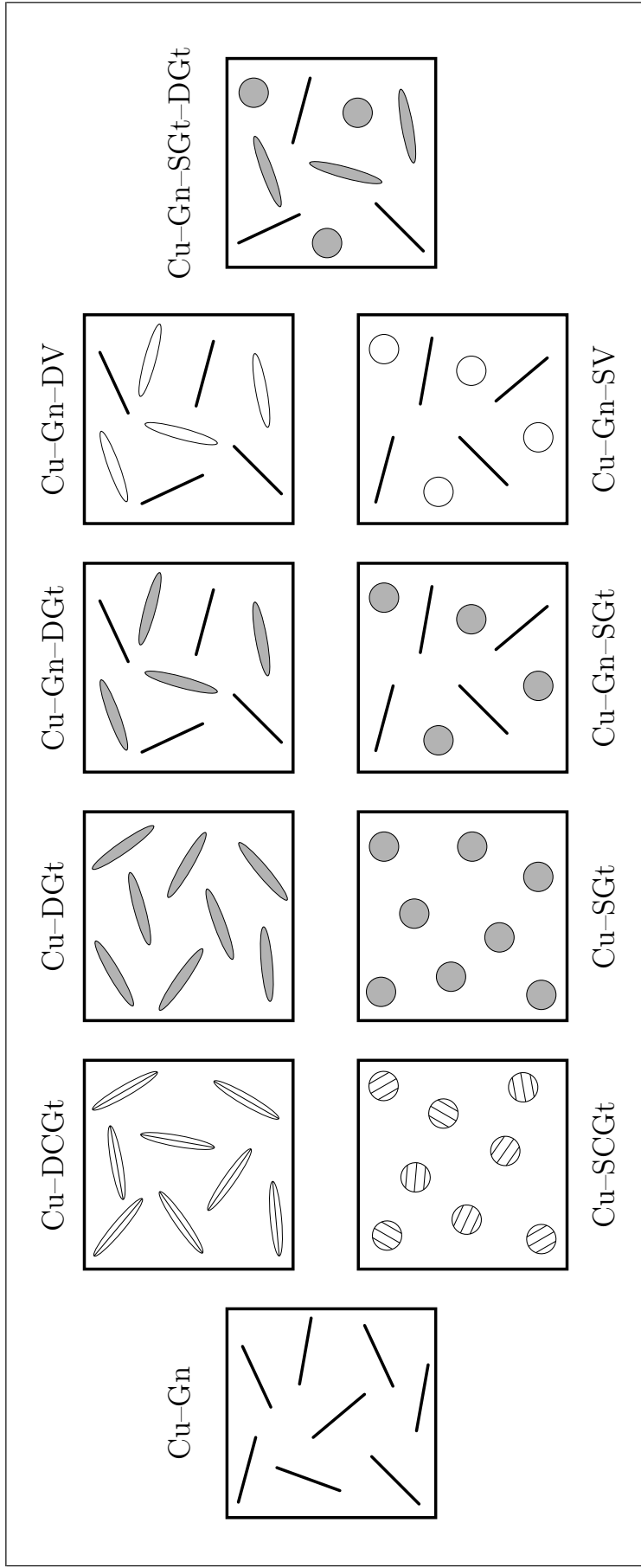


Fig. 2. Macroscopically isotropic composites considered in this work, see the list of inclusion types in Fig. 1.

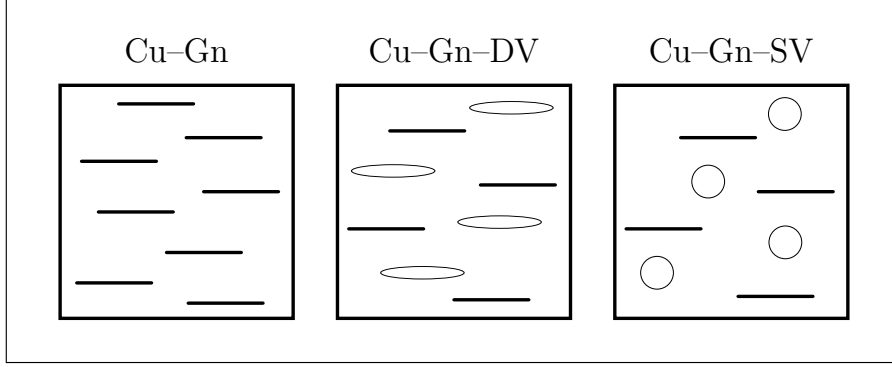


Fig. 3. Transversely isotropic composites with perfectly aligned disc-shaped inclusions considered in this work, see the list of inclusion types in Fig. 1.

the Eshelby concept [48]. Accordingly, the shape of every inclusion is approximated by an ellipsoid. All phases are thermoelastic and perfect bonding at the inclusion-matrix interfaces is assumed, hence the displacement and temperature are continuous at the interfaces.

The exposition below is aimed at providing the essential relationships of the micromechanical theory, and a detailed derivation is not attempted here. The details can be found, for instance, in [33–37].

A general equation for the effective elastic stiffness tensor of a multiphase composite is given by [49]

$$\bar{\mathbf{C}} = v_0 \mathbf{C}_0 \mathbf{A}_0 + \sum_n v_n \mathbf{C}_n \mathbf{A}_n, \quad (1)$$

where v_0 , \mathbf{C}_0 and \mathbf{A}_0 denote, respectively, the volume fraction, the elastic stiffness tensor and the strain concentration tensor of the matrix, while the corresponding quantities for the n -th type of inclusion are denoted by v_n , \mathbf{C}_n and \mathbf{A}_n . With the above notation, the total volume fraction of inclusions is defined as

$$v = \sum_n v_n = 1 - v_0 \quad (2)$$

Considering that the volume fractions sum up to unity and the strain concentration tensors average to the fourth-order unit tensor, Eq. (1) can be rewritten as [50, 51]

$$\bar{\mathbf{C}} = \mathbf{C}_0 + \sum_n v_n (\mathbf{C}_n - \mathbf{C}_0) \mathbf{A}_n. \quad (3)$$

The strain concentration tensors \mathbf{A}_n are fourth-order tensors that relate the average strain in each phase to the macroscopic strain. They are found by solving a microscopic problem and several analytical models that approximate \mathbf{A}_n have been developed, see e.g. [41, 46, 47, 52]. Two specific models which are applicable to multiphase composites are presented below and will be used in

the following.

For completeness, we first mention two simplest averaging schemes that provide upper and lower bounds on effective properties. The Voigt (upper) bound is obtained by assuming that the strain is uniform within the microstructure so that the strain concentration tensors reduce to unit tensors. As a result, the effective stiffness tensor is simply the volume average of the stiffness tensors of individual phases, which is evident from Eq. (1). On the contrary, averaging of the compliance tensors yields the Reuss (lower) bound which corresponds to the assumption of uniform stress.

A wide class of more accurate estimates of the effective properties is based on the Eshelby solution [48] of the problem of a single ellipsoidal inclusion in an infinite matrix. The simplest model valid for the non-dilute case is the Mori–Tanaka (MT) model [41, 46] in which each inclusion is embedded in an infinite medium having the properties of the matrix phase and experiences a far-field strain that is equal to the yet unknown average strain in the matrix. The strain concentration tensor is then found to be given by [46]

$$\mathbf{A}_n^{\text{MT}} = \mathbf{A}_n^{\text{dil}} \left[v_0 \mathbf{I} + \sum_k v_k \mathbf{A}_k^{\text{dil}} \right]^{-1}, \quad (4)$$

where \mathbf{I} is the fourth-order identity tensor and

$$\mathbf{A}_n^{\text{dil}} = \left[\mathbf{I} + \mathbf{S}_n (\mathbf{C}_0)^{-1} (\mathbf{C}_n - \mathbf{C}_0) \right]^{-1}, \quad (5)$$

is the strain concentration tensor for dilute inhomogeneities (which actually can be directly used in the dilute limit, say, for the total volume fraction of inclusions below 1% [53]).

In Eq. (5), \mathbf{S}_n is the so-called Eshelby tensor which follows from the solution of the Eshelby inclusion problem. The Eshelby tensor depends on the inclusion shape and on the properties of the matrix in the considered inclusion problem. The specific formulae for the components of the Eshelby tensor can be found in [33, 54].

In the case of the MT scheme, the Eshelby tensor depends on the known properties of the matrix phase, hence Eqs. (3), (4) and (5) specify explicit formulae for the effective elastic stiffness tensor. As a result, the MT scheme is relatively simple and is not numerically demanding. However, a direct application of the MT scheme to a multiphase composite may be problematic, see [47, 50, 55]. In particular, the effective elastic stiffness tensor may lack diagonal symmetry and may have an incorrect value at the dilute limit as well as at the unitary reinforcement concentration. Some of the inconsistencies of the MT scheme are not observed for special microstructures, for instance, for macroscopically

isotropic multiphase composites and for multiphase composites with perfectly aligned inclusions of similar shape.

The effective-medium-field (EMF) approximation proposed in [47] has been specifically developed in order to consistently treat multiphase composites. In the EMF scheme, it is assumed that each inclusion is embedded in an infinite medium with the yet unknown effective properties of the composite (as in the basic self-consistent scheme) and experiences a far-field strain equal to the yet unknown average strain in the matrix (as in the MT scheme). The strain concentration tensor is then found in the following form [47],

$$\mathbf{A}_n^{\text{EMF}} = \mathbf{A}_n^{\text{SC}} \left[v_0 \mathbf{I} + \sum_k v_k \mathbf{A}_k^{\text{SC}} \right]^{-1}, \quad (6)$$

and has the structure analogous to that of the MT scheme, Eq. (4), except that $\mathbf{A}_n^{\text{dil}}$ is now replaced by \mathbf{A}_n^{SC} that follows from the basic self-consistent (SC) scheme [52],

$$\mathbf{A}_n^{\text{SC}} = \left[\mathbf{I} + \mathbf{S}_n \bar{\mathbf{C}}^{-1} (\mathbf{C}_n - \bar{\mathbf{C}}) \right]^{-1}. \quad (7)$$

Now, in addition to the inclusion shape, the Eshelby tensor depends on the unknown effective properties of the composite. As a result, \mathbf{A}_n^{SC} depends on $\bar{\mathbf{C}}$ (both explicitly and through \mathbf{S}_n), hence Eqs. (3), (6) and (7) specify now a nonlinear equation for the effective stiffness tensor $\bar{\mathbf{C}}$ that must be solved numerically, for instance, using a fixed-point iteration method.

Following the route presented above for the effective elastic stiffness, the following formula for the tensor of the effective thermal expansion is obtained [37, 47],

$$\bar{\boldsymbol{\alpha}} = \boldsymbol{\alpha}_0 + \sum_n v_n (\boldsymbol{\alpha}_n - \boldsymbol{\alpha}_0) \mathbf{B}_n, \quad (8)$$

where $\boldsymbol{\alpha}_0$ and $\boldsymbol{\alpha}_n$ are the thermal expansion tensors of the matrix and the n -th phase, respectively, and \mathbf{B}_n is the stress concentration tensor, which is a fourth-order tensor that relates the average stress in each phase to the macroscopic stress. In the EMF approximation, the stress concentration tensor is given by

$$\mathbf{B}_n^{\text{EMF}} = \mathbf{B}_n^{\text{SC}} \left[v_0 \mathbf{I} + \sum_k v_k \mathbf{B}_k^{\text{SC}} \right]^{-1} \quad (9)$$

and

$$\mathbf{B}_n^{\text{SC}} = \left[\mathbf{I} + \bar{\mathbf{C}} (\mathbf{I} - \mathbf{S}_n) (\mathbf{D}_n - \bar{\mathbf{D}}) \right]^{-1}, \quad (10)$$

where $\mathbf{D}_n = \mathbf{C}_n^{-1}$ is the elastic compliance tensor of the n -th phase, and $\bar{\mathbf{D}} = \bar{\mathbf{C}}^{-1}$ is the effective elastic compliance tensor. The formulae corresponding to the MT scheme are analogous to those in Eqs. (9)–(10) with the effective elastic moduli $\bar{\mathbf{C}}$ and $\bar{\mathbf{D}}$ replaced by the elastic moduli of the matrix, respectively, \mathbf{C}_0 and \mathbf{D}_0 .

Finally, the effective thermal conductivity tensor is given by the general equation [36]

$$\bar{\boldsymbol{\kappa}} = \boldsymbol{\kappa}_0 + \sum_n v_n (\boldsymbol{\kappa}_n - \boldsymbol{\kappa}_0) \mathbf{K}_n, \quad (11)$$

where $\boldsymbol{\kappa}_0$ is the second-order thermal conductivity tensor of the matrix, $\boldsymbol{\kappa}_n$ is the thermal conductivity tensor of the n -th type of inclusions, and \mathbf{K}_n is the temperature gradient concentration tensor for the n -th type of inclusions. According to the considered micromechanical approximation scheme, the concentration tensor can be expressed via Eq. (4) and (6) with $\bar{\mathbf{C}}$, \mathbf{C}_0 and \mathbf{C}_n replaced by $\bar{\boldsymbol{\kappa}}$, $\boldsymbol{\kappa}_0$ and $\boldsymbol{\kappa}_n$, respectively, and with the appropriate Eshelby tensor corresponding to the heat conduction problem, see [56].

In general, non-spherical shape or anisotropic properties of inclusions may lead to anisotropy of effective properties. In that context, two general types of composites are considered in this work: composites with randomly oriented anisotropic inclusions and composites with anisotropic inclusions aligned along a preferential direction. In the later case, for perfectly aligned inclusions, the composite exhibits transverse isotropy at the macroscale, and the effective properties are then obtained by direct use of the equations presented above.

When the inclusions are randomly oriented, the composite is isotropic at the macroscale, and the effective properties are obtained by averaging over all the orientations of the inclusions. The general relation (3) takes then the form

$$\bar{\mathbf{C}} = \mathbf{C}_0 + \sum_n v_n \langle (\mathbf{C}_n - \mathbf{C}_0) \mathbf{A}_n \rangle, \quad (12)$$

where $\langle \boldsymbol{\Phi} \rangle$ denotes averaging of a tensorial quantity $\boldsymbol{\Phi}$ over the whole orientation space, see [57]. Following [35, 57, 58], using the rules of tensor calculus, the isotropic average of a fourth-order tensor $\boldsymbol{\Phi}$, satisfying the following symmetry relations $\Phi_{ijkl} = \Phi_{jikl} = \Phi_{ijlk}$, can be written as

$$\langle \boldsymbol{\Phi} \rangle = \Phi_h \boldsymbol{\Lambda}_h + \Phi_s \boldsymbol{\Lambda}_s, \quad (13)$$

where

$$\begin{aligned} (\boldsymbol{\Lambda}_h)_{ijkl} &= \frac{1}{3} \delta_{ij} \delta_{kl}, \\ (\boldsymbol{\Lambda}_s)_{ijkl} &= \frac{1}{2} (\delta_{ik} \delta_{jl} + \delta_{il} \delta_{jk}) - \frac{1}{3} \delta_{ij} \delta_{kl}, \\ \Phi_h &= \frac{1}{3} \Phi_{iijj}, \\ \Phi_s &= \frac{1}{5} \left(\Phi_{ijij} - \frac{1}{3} \Phi_{iijj} \right). \end{aligned}$$

As a result, apart from the symmetries of $\boldsymbol{\Phi}$, the average tensor $\langle \boldsymbol{\Phi} \rangle$ possesses also the major symmetry $\langle \boldsymbol{\Phi} \rangle_{ijkl} = \langle \boldsymbol{\Phi} \rangle_{klij}$.

The isotropic part of a second-order tensor $\boldsymbol{\phi}$ can be obtained using a similar averaging procedure,

$$\langle \boldsymbol{\phi} \rangle = \frac{1}{3} \phi_{ii} \mathbf{1}, \quad (14)$$

where $\mathbf{1}$ is the second-order identity tensor. This averaging procedure has been used to compute the isotropic effective thermal conductivities.

3 Application to copper–graphene composites

3.1 Assumptions and material properties

The classical estimates discussed in the previous section will now be applied to graphene-reinforced copper-matrix composites. As discussed in the Introduction, we assume that, due to the processing route, the composite includes not only graphene but also graphite inclusions and voids. Several assumptions are adopted in the present modelling. The first group of assumptions concerns the general applicability of the MT and EMF averaging schemes, see Section 2:

- (i) All inclusions are well approximated by an ellipsoidal shape so that the concept of the Eshelby inclusion [48] can be used.
- (ii) The inclusions are perfectly bonded to the matrix so that the displacements and temperature are continuous at the inclusion-matrix interfaces.
- (iii) Unless otherwise stated, the non-spherical and anisotropic inclusions are oriented randomly so that the composite is macroscopically isotropic.
- (iv) Disc-shaped inclusions are modelled as infinitely thin discs with the ellipsoid semi-axes satisfying $a_1 = a_2$ and $a_3 \rightarrow 0$. The corresponding Eshelby tensor is computed at the limit of $a_3 \rightarrow 0$, while the volume fraction is to be understood to correspond to small, but finite a_3 .

The second group of assumptions is related to the specific class of composites and inclusion types (see Figs. 1– 3) considered in this work:

- (v) Graphene (Gn) inclusions are modelled as infinitely thin discs.
- (vi) Two types of graphite inclusions are considered: crystalline graphite (CGt) with highly anisotropic properties and polycrystalline graphite (Gt) with isotropic properties. In both cases, the graphite inclusions are assumed in spherical shape or as infinitely thin discs.
- (vii) Voids of spherical (SV) or disc-like (DV) shape are modelled as inclusions with elastic stiffness and thermal conductivity equal to zero.
- (viii) All phases are assumed homogeneous with the properties specified in Tables 1–3, see the comments below.

In the examples reported below, the effective properties are provided as a function of the volume fraction of the inclusions ranging from 0 to 1. Clearly, the volume fraction of graphene in a composite material is not expected to exceed several percent. The results corresponding to higher volume fractions,

though not relevant in practical applications, are provided for completeness and to illustrate the relative dependencies between the actual effective properties of the composite and the reference properties of the matrix and individual inclusions.

For the isotropic composites, the predicted effective properties are reported below in terms of Young's modulus \bar{E} , coefficient of thermal expansion $\bar{\alpha}$ and thermal conductivity $\bar{\kappa}$. For the transversely isotropic composites, the predicted effective elastic properties are reported in terms of the directional Young's moduli \bar{E}_1 and \bar{E}_3 that correspond to a uniaxial stress state with the tension axis, respectively, normal and parallel to the axis of symmetry (aligned with the x_3 -axis). Relationships between the directional Young's moduli and the elastic constants for a transversely isotropic elastic material can be found in [34]. The effective in-plane and cross-plane thermal conductivities (respectively, $\bar{\kappa}_{11}$ and $\bar{\kappa}_{33}$) and the effective in-plane and cross-plane thermal expansion coefficients (respectively, $\bar{\alpha}_{11}$ and $\bar{\alpha}_{33}$) are simply equal to the components of the corresponding second-order effective tensors $\bar{\boldsymbol{\kappa}}$ and $\bar{\boldsymbol{\alpha}}$.

In the present modelling, the nano-effects are not considered, and graphene is treated as a classical anisotropic solid. Since graphene exhibits isotropic in-plane properties (due to the hexagonal lattice), the adequate anisotropy class is the transverse isotropy. The in-plane properties of graphene are well characterized, but the out-of-plane properties are not known. In fact, the out-of-plane properties can be largely controlled by the interfacial phenomena which are not considered in this work. The properties of a transversely isotropic solid that represents graphene, as considered below, should thus be treated as effective properties characterizing the overall behaviour of the graphene and the graphene-matrix interfaces.

A simplified approach is adopted here to describe the out-of-plane elastic properties of graphene. We start by noting that the in-plane elastic modulus of graphene, typically reported to be of the order of 1000 GPa [2], is very close to the in-plane modulus of crystalline graphite. For instance, for the elastic constants reported in [23], the in-plane elastic modulus of crystalline graphite is equal to 1025 GPa. The crystalline graphite is transversely isotropic and exhibits high anisotropy with the ratio of cross-plane elastic modulus E_3 to the in-plane modulus E_1 equal to 0.035. The elastic stiffness tensor of crystalline graphite, denoted by \mathbf{C}^{CGt} , is thus adopted as the lower bound for the stiffness tensor of graphene. As the upper bound, we adopt the stiffness tensor, denoted by $\mathbf{C}^{\text{isoGn}}$, corresponding to an isotropic solid with the Young's modulus and Poisson's ratio equal to the respective in-plane moduli of crystalline graphite equal to 1025 GPa and 0.16, respectively [23]. Finally, in the examples below, we study the effect of out-of-plane properties of graphene by considering the

Table 1

Elastic constants and thermal expansion coefficients of graphene treated as a transversely isotropic solid, see the parametrization in Eq. (15). The case of $\eta = 0$ corresponds to crystalline graphite.

η	Elastic constants [GPa]						Thermal expansion coeff. [$10^{-6}/\text{K}$]		
	c_{11}	c_{12}	c_{13}	c_{33}	c_{44}	E_3/E_1	$\alpha_{11} = \alpha_{22}$	α_{33}	
0	1060	180	15	36.5	4.5	0.035	-1	30	
0.1	1064	184	35	142	48	0.14	-1.7	26	
1	1097	217	217	1097	440	1	-8	-8	

Table 2

Thermal conductivities in [W/mK] of graphene (Gn) and crystalline graphite (CGt), see text.

	$\kappa_{11} = \kappa_{22}$	κ_{33}
Gn	5000	{5, 50, 500, 5000}
CGt	2000	10

following parametrization of the elastic stiffness tensor,

$$\mathbf{C}^{\text{Gn}} = (1 - \eta)\mathbf{C}^{\text{CGt}} + \eta\mathbf{C}^{\text{isoGn}}, \quad (15)$$

so that $\eta = 0$ corresponds to the crystalline graphite with $E_3/E_1 = 0.035$ and $\eta = 1$ corresponds to $E_3/E_1 = 1$. Additionally, an intermediate value of $\eta = 0.1$ is considered which corresponds to $E_3/E_1 = 0.14$.

The elastic constants used for graphene according to the parametrization (15) are provided in Table 1. The coefficients of thermal expansion are treated analogously, and the corresponding parameters are also provided in Table 1.

The in-plane thermal conductivity κ_{11} of the pristine, suspended graphene has been reported in the range between 4840 and 5300 W/mK [1], and the value of 5000 W/mK is adopted in this work. As the out-of-plane conductivity is concerned, several values of κ_{33} are used in the present computations. The case of $\kappa_{33}/\kappa_{11} = 1$, corresponding to isotropic thermal conductivity, is adopted as an upper bound, but more realistic, lower values of κ_{33}/κ_{11} are also considered, see Table 2. In-plane and out-of-plane thermal conductivities of crystalline graphite [59] are also provided in Table 2. Note that thermal anisotropy of crystalline graphite is very high ($\kappa_{33}/\kappa_{11} = 0.005$), and it is expected that graphene exhibits a high anisotropy as well.

To complete specification of material parameters used in the present study, the parameters of isotropic polycrystalline graphite (Gt) and isotropic polycrys-

Table 3

Properties of isotropic polycrystalline graphite (Gt) and isotropic copper matrix (Cu).

	Gt	Cu
Young’s modulus [GPa]	10	120
Poisson’s ratio	0.16	0.34
Thermal expansion coeff. [$10^{-6}/\text{K}$]	2.9	17
Thermal conductivity [W/mK]	100	400

talline copper are provided in Table 3. The properties adopted for copper are representative for pure copper [60,61]. In particular, the thermal conductivity of 400 W/mK is relatively high, and noticeably lower values can be encountered depending on the microstructure and purity. At the same time, the properties of isotropic polycrystalline graphite are even more sensitive to the variations in microstructure and quality. Young’s modulus at room temperature is typically reported between 4 and 16 GPa and the thermal conductivity between 60 and 200 W/mK [59,62–64], so that intermediate values have been adopted in the present study (Table 3). In any case, those properties are at least one order of magnitude lower than the corresponding in-plane properties of crystalline graphite, which is due to the very high anisotropy of graphite.

3.2 *Micromechanical predictions for macroscopically isotropic two-phase composites*

We start by examining a perfect isotropic two-phase copper–graphene composite, i.e., a composite with no graphite inclusions and no voids. This reference case is actually the theoretical limit of what can be achieved by adding randomly oriented graphene to a copper matrix. Here and below, the effective properties of the composite are normalized by the corresponding properties of the matrix, denoted by ‘0’ in the subscript, and representing the reference material without any inclusions.

The normalized effective Young’s modulus \bar{E}/E_0 , thermal expansion coefficient $\bar{\alpha}/\alpha_0$ and thermal conductivity $\bar{\kappa}/\kappa_0$ are shown in Fig. 4 as a function of the volume fraction v_{Gn} of graphene. Here and throughout the paper, the predictions of the MT model are denoted by solid lines and those of the EMF model by dashed lines. We recall that the results corresponding to high volume fractions are reported here even though the physically sound range of volume fractions may be exceeded.

It is seen in Fig. 4 that the isotropic effective properties depend strongly on

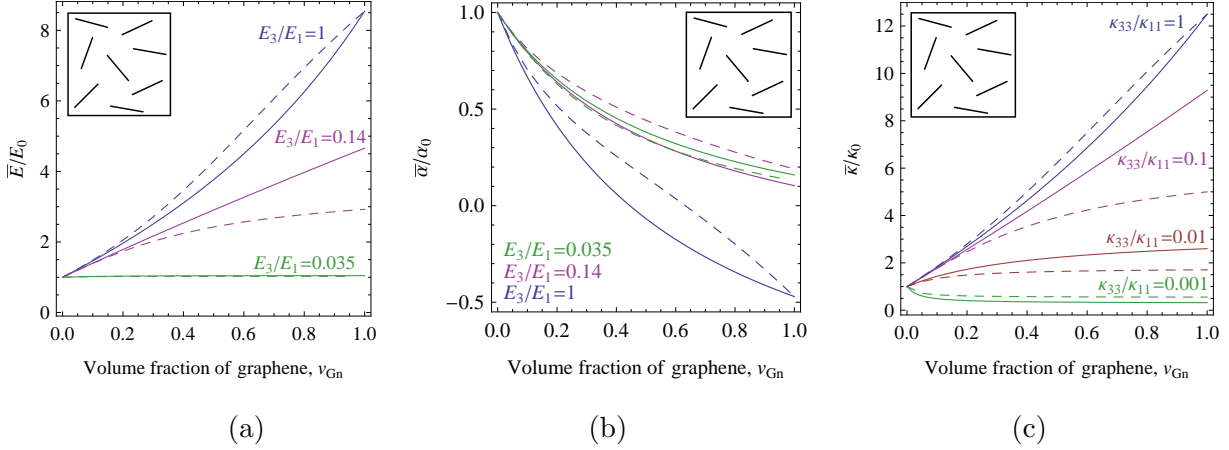


Fig. 4. Isotropic copper–graphene composite: influence of the out-of-plane properties of graphene (E_3 and κ_{33}) on (a) effective Young’s modulus, (b) coefficient of thermal expansion and (c) thermal conductivity. Here and throughout the paper, solid lines correspond to the MT model, dashed lines correspond to the EMF model.

the out-of-plane properties of the graphene inclusions, even though the inclusions are disc-shaped ($a_3 \rightarrow 0$). In fact, the stiffening effect due to the high in-plane stiffness of graphene disappears for $E_3/E_1 = 0.035$, Fig. 4a. Similarly, enhancement of the effective thermal conductivity vanishes for κ_{33}/κ_{11} between 0.01 and 0.001, Fig. 4c.

In order to illustrate the performance of graphite as a reinforcement phase, the effective properties of copper–graphite composites are provided in Fig. 5 for crystalline graphite (CGt) and in Fig. 6 for polycrystalline graphite (Gt). The effect of inclusion shape is also illustrated in Figs. 5 and 6 by considering spherical inclusions (SCGt and SGt) and randomly oriented disc inclusions with $a_3 \rightarrow 0$ (DCGt and DGt). In the latter case, the symmetry axis of transversely isotropic crystalline graphite is assumed normal to the discs.

In the case of crystalline graphite (CGt), the effective Young’s modulus does not change significantly with increasing volume fraction of graphite for both spherical and disc-shaped inclusions, Fig. 5a. At the same time, the effect of inclusion shape on the effective thermal conductivity is significant, Fig. 5c. For disc-shaped inclusions (DCGt), the thermal conductivity decreases by 50% for $v_{\text{CGt}} = 0.2$, while it increases by approximately 15% for the same volume fraction of spherical inclusions. Note that the performance of crystalline graphite is similar to that of graphene modelled as a highly anisotropic material. This, of course, is a result of the assumptions adopted in Section 3.1.

In the case of polycrystalline graphite (Gt), Fig. 6, both the elastic modulus and the thermal conductivity decrease with increasing volume fraction of graphite both for spherical and disc-shaped inclusions, while the effect of shape of inclusions is more significant in the case of elastic modulus. Referring to the multiphase composites discussed below, it is thus expected that polycrys-

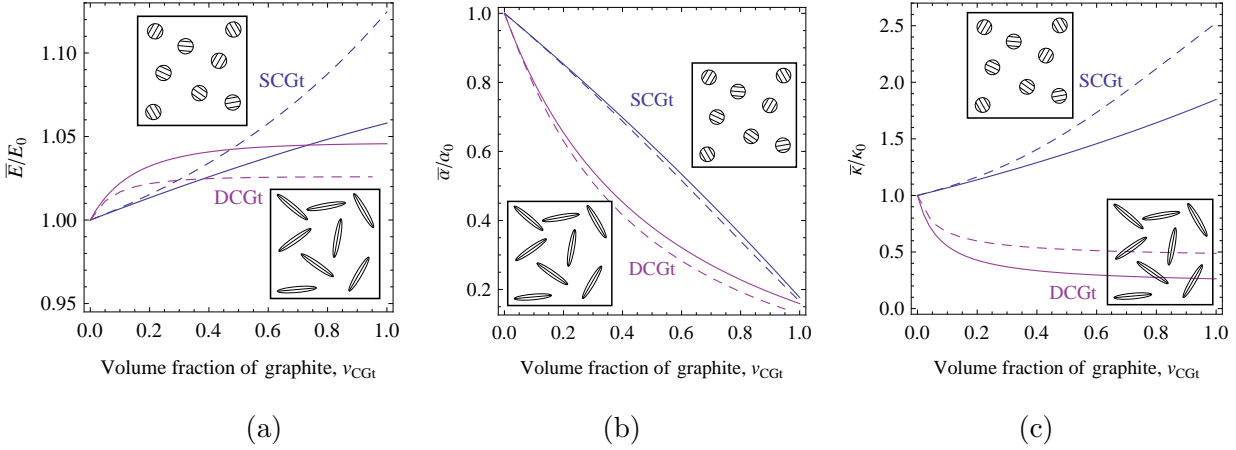


Fig. 5. Isotropic copper–crystalline graphite composite: influence of the inclusion shape on (a) effective Young’s modulus, (b) coefficient of thermal expansion and (c) thermal conductivity.

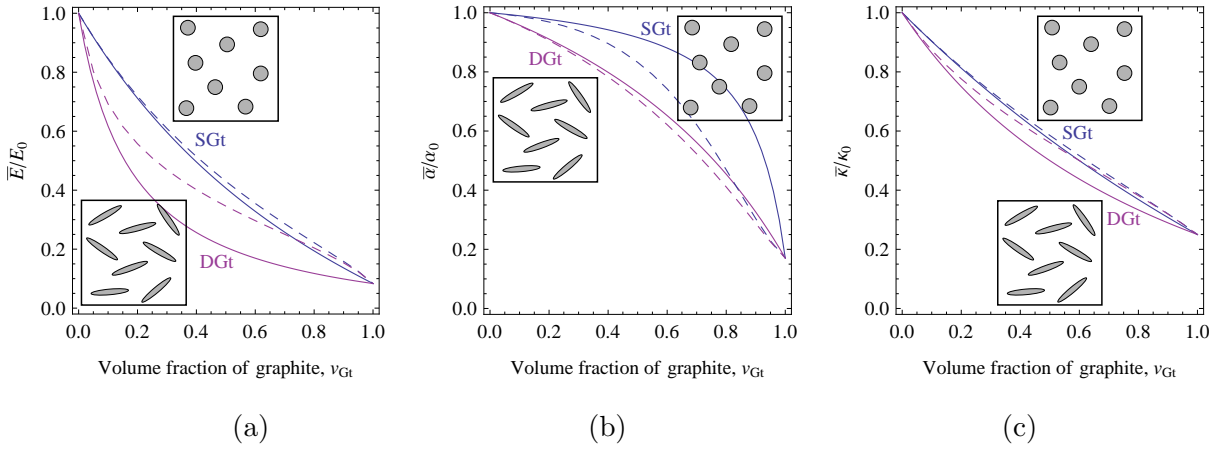


Fig. 6. Isotropic copper–polycrystalline graphite composite: influence of the inclusion shape on (a) effective Young’s modulus, (b) coefficient of thermal expansion and (c) thermal conductivity.

talline graphite would lower the thermoelastic properties of a copper–graphene composite contaminated by polycrystalline graphite.

In all cases studied above, the effective coefficient of thermal expansion decreases with increasing volume fraction of graphene and graphite, which may be beneficial in some applications. This is expected in view of the low, or even negative, thermal expansion coefficient of graphene and graphite. The most significant decrease is predicted for graphene with $\eta = 1$, i.e., for isotropic elastic moduli and isotropic thermal expansion, see Table 1. For more realistic properties of graphene and for graphite, the decrease is noticeably lower.

As it is well known, the difference between the predictions of the two averaging schemes (MT and EMF) is not much pronounced at low volume fractions of inclusions. Depending on the specific composite considered, the MT scheme

appears sufficiently accurate when the volume fraction of inclusions does not exceed several percent. Otherwise, the EMF scheme would be preferable as it is more reliable, but also it is more complex and more demanding.

3.3 *Effective properties of macroscopically isotropic multiphase composites*

In this section, we study the effective properties of isotropic multiphase copper–graphene composites. Specifically, we study the effect of graphite that may be present in a composite material as a result of imperfect processing, as discussed in detail in the Introduction. The effect of voids, which constitute another kind of imperfection of composites produced, for instance, by powder metallurgy, is also considered using the same modelling approach.

Below, we only report the results corresponding to copper–graphene composites containing polycrystalline graphite since the influence of crystalline graphite is significantly less pronounced. Actually, as illustrated in Section 3.2, the properties of a copper–crystalline graphite composite do not differ much from those of a copper–graphene composite when realistic out-of-plane properties of graphene are adopted.

Figure 7 shows the normalized effective thermal conductivity of a copper–matrix composite with graphene and polycrystalline graphite inclusions, the latter having spherical or disc-like shape. The thermal conductivity is shown as a function of the total volume fraction of inclusions for three fixed ratios of the graphite-to-graphene content. The results for a two-phase copper–graphene composite are also provided as a reference. The out-of-plane thermal conductivity of graphene, which has a significant effect on the effective conductivity, see Fig. 4c, is adopted here as $\kappa_{33}/\kappa_{11} = 0.01$, which is assumed to be a reasonably realistic value.

As expected, the effective thermal conductivity decreases with increasing relative content of graphite. The effect of the shape of graphite inclusions is not much pronounced, and the disc-shaped inclusions result in a somewhat higher reduction than the spherical inclusions. This is consistent with the results obtained for a two-phase copper–polycrystalline graphite composite, Fig. 6c.

The effect of polycrystalline graphite and inclusion shape is further illustrated in Fig. 8. Here, a copper–graphene composite is considered which additionally contains two families of polycrystalline graphite inclusions, namely spherical and disc-shaped inclusions. The diagrams in Fig. 8 present contour plots of normalized effective properties at a fixed total volume fraction of inclusions. The position within the triangular domain specifies the relative volume fraction of the three inclusion types (Gn, SGt, DGt), and the colour denotes the corresponding value of the parameter according to the scale provided in the

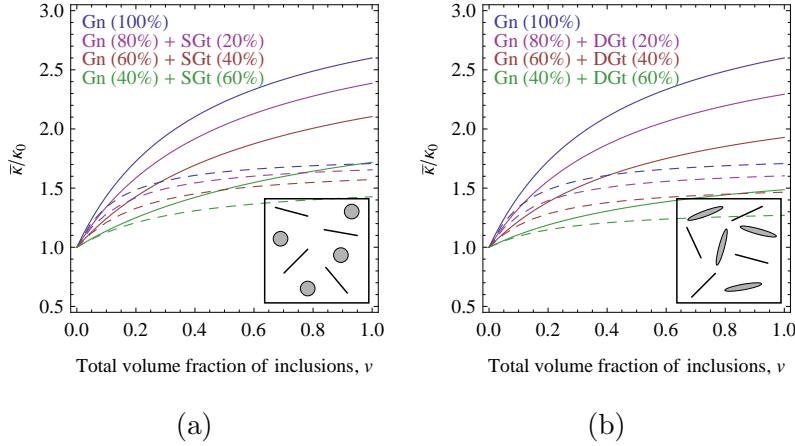


Fig. 7. Effective thermal conductivity of a three-phase composite with graphene ($\kappa_{33}/\kappa_{11} = 0.01$) and polycrystalline graphite inclusions, the latter having (a) spherical or (b) disc-like shape.

respective legend. The vertices correspond to two-phase composites containing only one type of inclusions, and each vertex is labelled accordingly along with the corresponding value of the parameter. The edges and the interior of the triangular domain correspond, respectively, to three- and four-phase composites, and the relative volume fraction of each phase is determined by the proximity to the corresponding vertex.

It is seen that the isolines in Fig. 8 are approximately straight, parallel and equally spaced. This means that the dependence of the effective properties on the relative volume fractions of the inclusions is approximately linear in the considered range of the total volume fraction ν . Accordingly, the effective property of a multiphase composite can be obtained with a good approximation as a linear combination of the values corresponding to the respective two-phase composites.

Finally, the effect of voids on the effective thermal conductivity of an isotropic copper–graphene composite is illustrated in Fig. 9. Here, the effect of void shape is very pronounced, which is a well-known property [35]. In fact, the effective thermal conductivity decreases by 10–15% for 10% volume fraction of spherical voids, while just 0.1% volume fraction of disc-shaped voids results in a reduction by 60%.

3.4 Effective properties of transversely isotropic composites

It has been shown in the preceding subsections that the enhancement of thermomechanical properties in an isotropic copper–graphene composite is largely limited due to random orientation of graphene in the matrix. Clearly, the extraordinary (in-plane) properties of graphene can be exploited more effec-

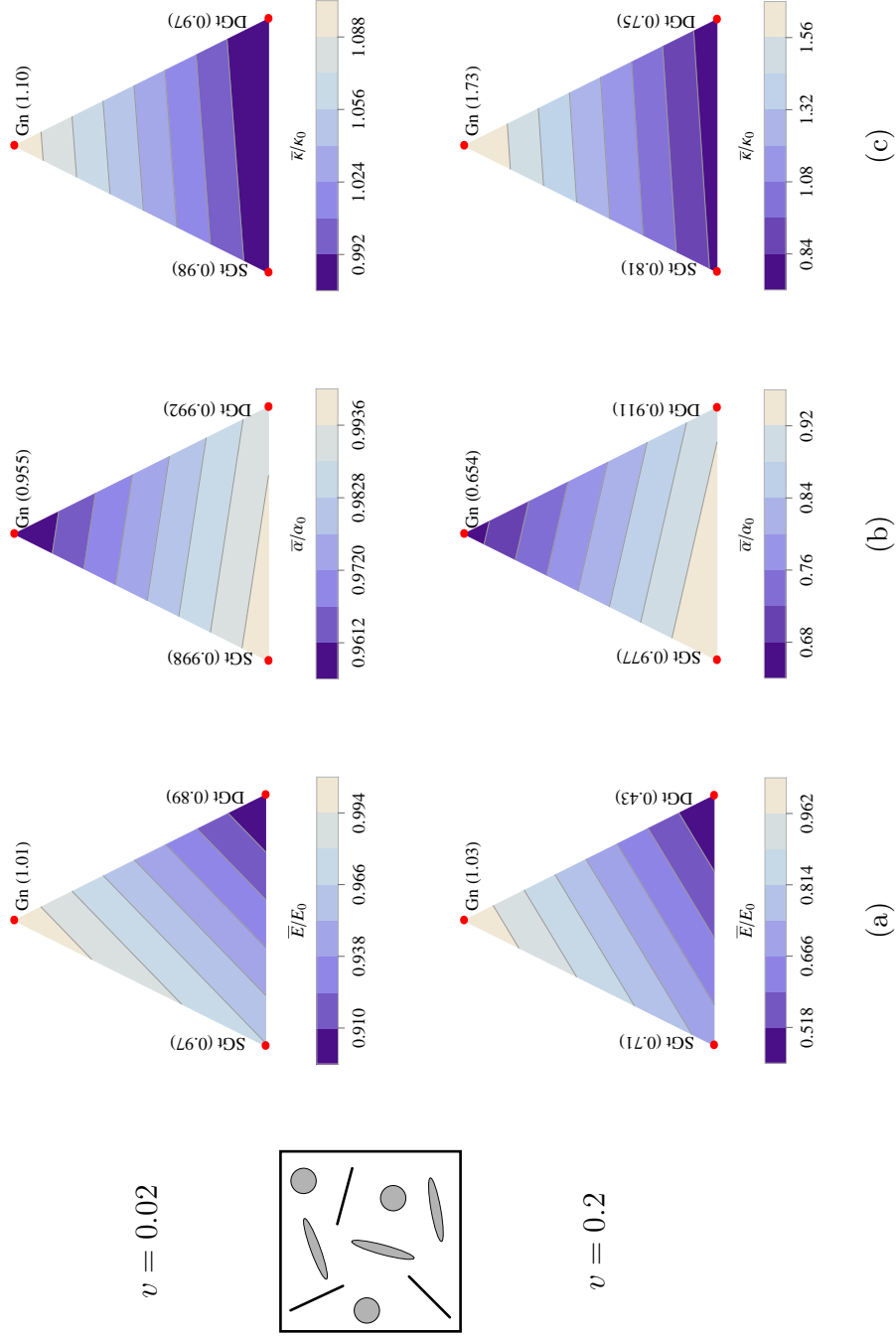


Fig. 8. Contour plots of the effective properties for a multiphase Cu-Gn-SGt-DGt composite for a fixed total volume fraction of inclusions equal to $v = 0.02$ (top) and $v = 0.2$ (bottom): (a) Young's modulus, (b) coefficient of thermal expansion and (c) thermal conductivity (predictions of the MT model; properties of graphene correspond to $E_3/E_1 = 0.035$ and $\kappa_{33}/\kappa_{11} = 0.01$).

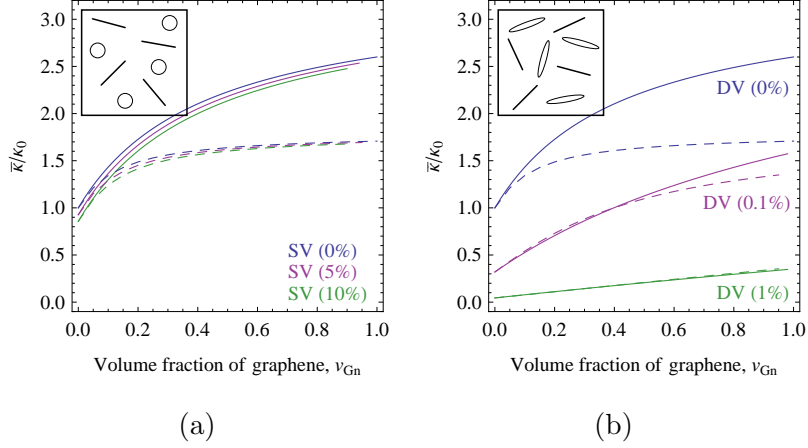


Fig. 9. Effect of voids on the effective thermal conductivity for a copper–graphene composite ($\kappa_{33}/\kappa_{11} = 0.01$). Voids are modelled as (a) spheres (SV) and (b) discs (DV).

tively by arranging graphene platelets along a preferential direction. Accordingly, in this subsection, we study a copper–graphene composite in which all graphene discs are parallel so that the material exhibits transverse isotropy at the macroscale.

The in-plane and cross-plane effective properties of a transversely isotropic copper–graphene composite are shown in Fig. 10. It is seen that the in-plane Young’s modulus and the in-plane thermal conductivity do not depend on the out-of-plane properties assumed for graphene. Of course, the cross-plane properties are controlled by the out-of-plane properties of graphene, and here the effect is very significant.

The dependence of the effective in-plane Young’s modulus and thermal conductivity on the volume fraction of graphene is approximately linear, hence, as expected, the effective in-plane properties can be significantly improved by orienting the graphene inclusions.

The effect of voids on the effective thermal conductivity of a transversely isotropic copper–graphene composite is shown in Fig. 11 for $\kappa_{33}/\kappa_{11} = 0.01$ assumed for graphene. Spherical voids have a small effect on both the in-plane and cross-plane thermal conductivity, see Fig. 11a. This is consistent with the results shown in Fig. 9a for an isotropic composite. The disc-shaped voids, which are here assumed to be parallel to the graphene platelets, have a significant effect on the cross-plane conductivity, similar to that illustrated in Fig. 9b, while the in-plane conductivity is not affected.

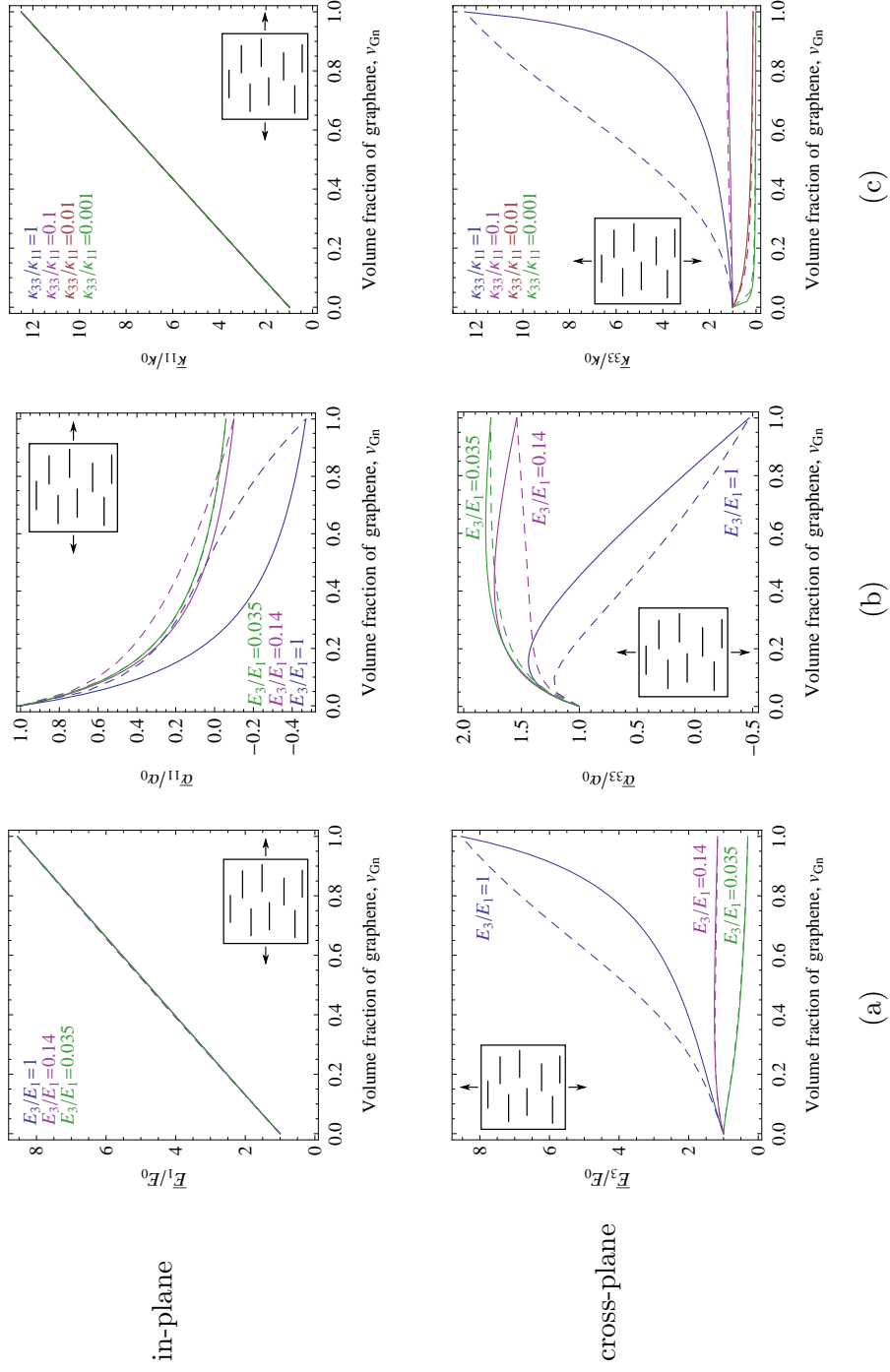


Fig. 10. In-plane (top) and cross-plane (bottom) effective properties of a transversely isotropic copper-graphene composite: (a) Young's modulus, (b) coefficient of thermal expansion and (c) thermal conductivity.

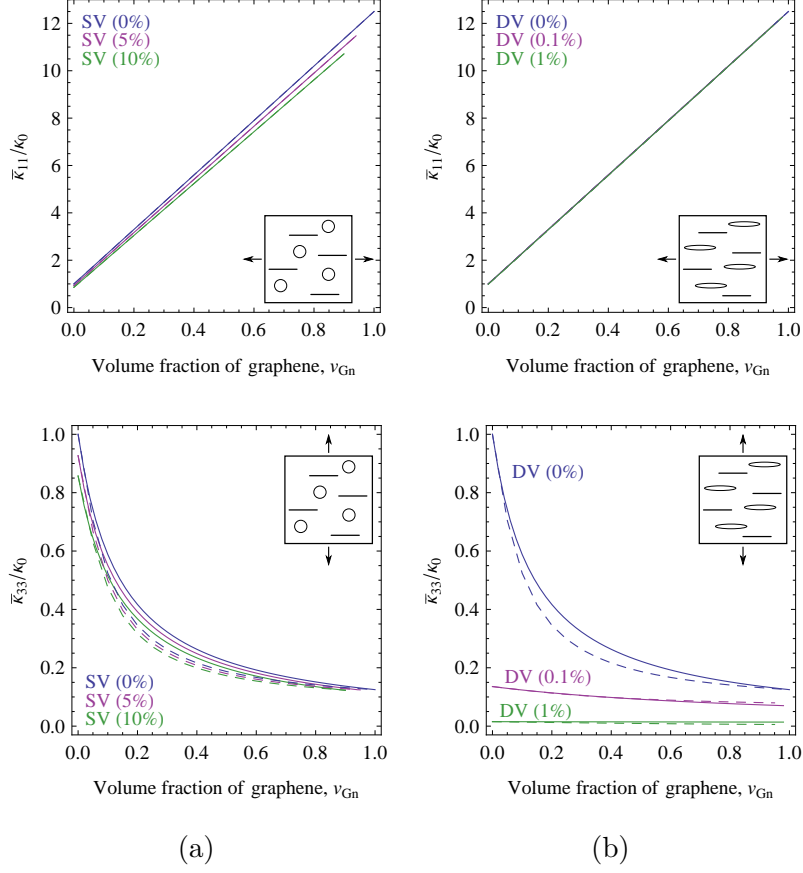


Fig. 11. In-plane (top) and cross-plane (bottom) effective thermal conductivity of a transversely isotropic copper–graphene composite with (a) spherical and (b) disc-shaped voids.

3.5 Comparison to available experimental data

Experimental measurements of the effective thermoelastic properties of copper–graphene composites are scarce. Actually, we were only able to find two relevant experimental works. These results and the associated micromechanical predictions are discussed below.

Chu and Jia [19] reported the effective Young’s modulus of a copper–graphene composite produced by a typical powder metallurgy process: milling of a mixture of copper powder and graphene nano-platelets, followed by compaction and sintering. The processing route leads to a random distribution of graphene platelets and isotropic properties of the composite. The measured Young’s modulus is shown in Fig. 12 as a function of the volume fraction of graphene. Included in Fig. 12 are also the micromechanical predictions which are computed here using the actual Young’s modulus of copper matrix equal to 76 GPa, as measured in [19]. The difference with respect to the typical value of 120 GPa may result, for instance, from residual porosity after sinter-

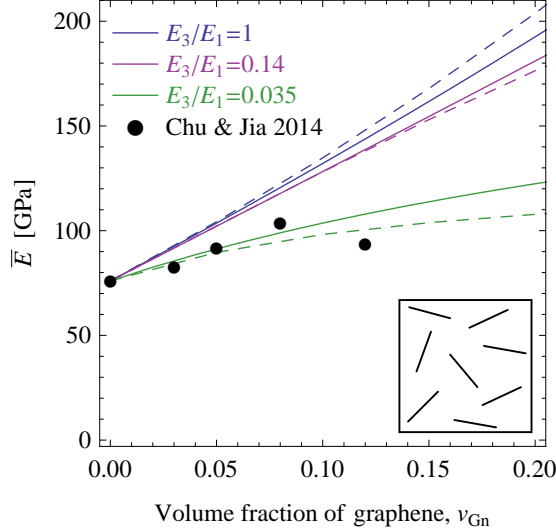


Fig. 12. Effective Young’s modulus of an isotropic copper–graphene composite: micromechanical predictions compared to experimental data of Chu and Jia [19].

ing. A reasonably good agreement of the theoretical predictions with experiment is observed for the out-of-plane properties of graphene corresponding to $E_3/E_1 = 0.035$, i.e., for $\eta = 0$ in the parametrization (15).

Note that the experimental Young’s modulus measured for the highest volume fraction $v_{\text{Gn}} = 0.12$ does not fit the general trend. This has been associated in [19] to an increased aggregation of graphene platelets observed at higher volume fractions, which results in formation of pores and reduction of the effective modulus. In fact, a noticeable decrease of relative density has been observed for $v_{\text{Gn}} = 0.12$, cf. [19].

The second example is concerned with the effective thermal conductivity of an electrochemically codeposited copper–graphene composite [27,28]. Samples of Cu–Gn composite were electrochemically codeposited on oxygen-free high-conductivity copper foils from a bath containing graphene oxide suspension in a solution of technical grade CuSO_4 in distilled water. As stated in [27], graphene is distributed uniformly in the composite films, thus the composite is assumed to be macroscopically isotropic.

Thermal conductivity of the copper–graphene composite, measured by the $3\text{-}\omega$ method [65], is shown in Fig. 13 as a function of the volume fraction of graphene. The corresponding micromechanical predictions, also shown in Fig. 13, have been obtained for the thermal conductivity of copper matrix equal to 380 W/mK , as reported in [27]. The experimental data are close to the predictions obtained for the out-of-plane conductivity of graphene specified by the ratio $\kappa_{33}/\kappa_{11} = 0.005$. Interestingly, this value of the κ_{33}/κ_{11} ratio is equal to the ratio of the out-of-plane to the in-plane thermal conductivity of crystalline graphite, cf. Table 2.

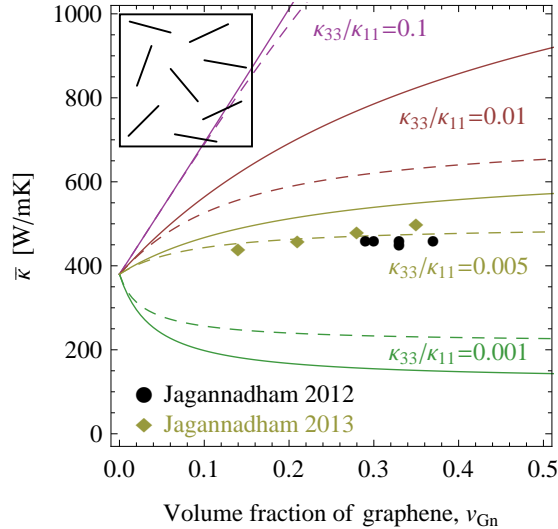


Fig. 13. Effective thermal conductivity of a copper–graphene composite: micromechanical predictions compared to experimental data of Jagannadham [27, 28].

4 Conclusion

The Mori–Tanaka method and the effective-medium-field approximation have been used to estimate the effective thermoelastic properties of multiphase copper–graphene composites. It has been assumed that the composite additionally contains particles of graphite and voids as a result of imperfect processing. The influence of those undesired inclusions has been investigated quantitatively, and it has been shown that the expected enhancement of the effective properties can be significantly reduced.

The main simplification adopted in the present modelling is that graphene has been treated as an ordinary anisotropic thermoelastic material so that the nano-effects are not included in the analysis. However, the adopted approach allowed us to study the influence of the out-of-plane properties of graphene which are expected to be significantly lower than its exceptional in-plane properties, the former being also less recognized.

The micromechanical predictions obtained for isotropic composites with randomly oriented graphene platelets indicate that the out-of-plane properties of graphene strongly influence the effective properties. In particular, assuming that graphene is highly anisotropic with the out-of-plane properties specified by the ratios E_3/E_1 and κ_{33}/κ_{11} corresponding to crystalline graphite (equal to 0.035 and 0.005, respectively), the effective Young’s modulus and the effective thermal conductivity have been found to be essentially unaffected by the increasing volume fraction of graphene. This suggests that the achievable enhancement of the elastic modulus and thermal conductivity of copper is limited for randomly oriented graphene inclusions, as confirmed by the exper-

imental data analyzed in Section 3.5. Also, the crucial role of the out-of-plane properties of graphene calls for a reliable characterization of those properties.

Clearly, regardless of the actual anisotropy of graphene, significant enhancement of directional properties is possible in a macroscopically anisotropic composite with graphene platelets arranged parallel to a specified plane. The effective properties of the corresponding transversely anisotropic composites have also been estimated, including the analysis of the effect of void shape and volume fraction.

The study reported in the present paper shows that the adopted micromechanical approach can serve as an efficient tool for a fast and robust estimation of the effective properties of graphene-based metal-matrix composites. Of course, the micromechanical predictions can be regarded reliable only if the properties of the graphene itself are properly identified, particularly the out-of-plane properties, as discussed above. The feasibility of the present approach is confirmed by the comparison of the predictions to available experimental data, as reported in Section 3.5.

Acknowledgement

This work was partially supported by the National Science Center (NCN) through the grant No. 2013/09/B/ST8/03320 and by the Centre of Excellence and Innovation of Composite Materials (CDIMK) at IPPT.

References

- [1] A. A. Balandin, S. Ghosh, W. Bao, I. Calizo, D. Teweldebrhan, F. Miao, C. N. Lau, Superior thermal conductivity of single-layer graphene, *Nano Letters* 8 (2008) 902–907.
- [2] C. Lee, X. Wei, J. W. Kysar, J. Hone, Measurement of the elastic properties and intrinsic strength of monolayer graphene, *Science* 321 (2008) 385–388.
- [3] M. Terrones, A. R. Botello-Méndez, J. Campos-Delgado, F. López-Urias, Y. I. Vega-Cantú, F. J. Rodríguez-Macias, A. L. Elias, E. Muñoz Sandoval, A. G. Cano-Márquez, J. C. Charlier, H. Terrones, Graphene and graphite nanoribbons: morphology, properties, synthesis, defects and applications, *Nano Today* 5 (2010) 351–372.
- [4] J. H. Seol, I. Jo, A. L. Moore, L. Lindsay, Z. H. Aitken, M. T. Pettes, X. Li, Z. Yao, R. Huang, D. Broido, N. Mingo, R. S. Ruoff, L. Shi, Two-dimensional phonon transport in supported graphene, *Science* 328 (2010) 213–216.

- [5] L. Chen, S. Kumar, Thermal transport in graphene supported on copper, *Journal of Applied Physics* 112 (2012) 043502.
- [6] K. Chu, C. Jia, W. Li, Effective thermal conductivity of graphene-based composites, *Applied Physics Letters* 101 (2012) 121916.
- [7] E. Pop, V. Varshney, A. K. Roy, Thermal properties of graphene: fundamentals and applications, *Materials Research Society* 37 (2012) 1273–1281.
- [8] J. Wang, Z. Li, G. Fan, H. Pan, Z. Chen, D. Zhang, Reinforcement with graphene nanosheets in aluminum matrix composites, *Scripta Materialia* 66 (2012) 594–597.
- [9] Y. Zhang, C. Pan, Measurements of mechanical properties and number of layers of graphene from nano-indentation, *Diamond & Related Materials* 24 (2012) 1–5.
- [10] J. D. Renteria, D. L. Nika, A. A. Balandin, Graphene thermal properties: applications in thermal management and energy storage, *Applied Sciences* 4 (2014) 525–547.
- [11] A. K. Geim, K. S. Novoselov, The rise of graphene, *Nature Materials* 6 (2007) 183–191.
- [12] T. Kuilla, S. Bhadra, D. Yao, N. H. Kim, S. Bose, J. H. Lee, Recent advances in graphene based polymer composites, *Progress in Polymer Science* 35 (2010) 1350–1375.
- [13] J. Du, H. M. Cheng, The fabrication, properties, and uses of graphene/polymer composites, *Macromolecular Chemistry and Physics* 213 (2012) 1060–1077.
- [14] V. Goyal, A. A. Balandin, Thermal properties of the hybrid graphene-metal nano-micro-composites: Applications in thermal interface materials, *Applied Physics Letters* 100 (2012) 073113.
- [15] S. F. Bartolucci, J. Paras, M. A. Rafiee, J. Rafiee, S. Lee, D. Kapoor, N. Koratkar, Graphene-aluminum nanocomposites, *Materials Science and Engineering A* 528 (2011) 7933–7937.
- [16] L. Y. Chen, H. Konishi, A. Fehrenbacher, C. Ma, J. Q. Xu, H. Choi, H. F. Xu, F. E. Pfefferkorn, X. C. Li, Novel nanoprocessing route for bulk graphene nanoplatelets reinforced metal matrix nanocomposites, *Scripta Materialia* 67 (2012) 29–32.
- [17] T. S. Koltsova, L. I. Nasibulina, I. V. Anoshkin, V. V. Mishin, E. I. Kauppinen, O. V. Tolochko, A. G. Nasibulin, New hybrid copper composite materials based on carbon nanostructures, *Journal of Materials Science and Engineering B* 2 (2012) 240–246.
- [18] J. Hwang, T. Yoon, S. H. Jin, J. Lee, T. S. Kim, S. H. Hong, S. Jeon, Enhanced mechanical properties of graphene/copper nanocomposites using a molecular-level mixing process, *Advanced Materials* 25 (2013) 6724–6729.

- [19] K. Chu, C. Jia, Enhanced strength in bulk graphene–copper composites, *Physica Status Solidi A* 211 (2014) 184–190.
- [20] W. J. Kim, T. J. Lee, S. H. Han, Multi-layer graphene/copper composites: Preparation using high-ratio differential speed rolling, microstructure and mechanical properties, *Carbon* 69 (2014) 55–65.
- [21] M. Li, H. Che, X. Liu, S. Liang, H. Xie, Highly enhanced mechanical properties in Cu matrix composites reinforced with graphene decorated metallic nanoparticles, *Journal of Materials Science* 49 (2014) 3725–3731.
- [22] B. Partoens, F. M. Peeters, From graphene to graphite: electronic structure around the K point, *Physical Review B* 74 (2006) 075404.
- [23] B. T. Kelly, *Physics of Graphite*, Applied Science Publishers, London, 1981.
- [24] S. W. Chang, A. K. Nair, M. J. Buehler, Geometry and temperature effects of the interfacial thermal conductance in copper– and nickel–graphene nanocomposites, *Journal of Physics: Condensed Matter* 24 (2012) 1–6.
- [25] S. Stankovich, D. A. Dikin, G. H. B. Dommett, K. M. Kohlhaas, E. J. Zimney, E. A. Stach, R. D. Piner, S. T. Nguyen, R. S. Ruoff, Graphene-based composite materials, *Nature* 442 (2006) 282–286.
- [26] X. Y. Ji, Y. P. Cao, X. Q. Feng, Micromechanics prediction of the effective elastic moduli of graphene sheet-reinforced polymer nanocomposites, *Modelling and Simulation in Materials Science and Engineering* 18 (2010) 1–16.
- [27] K. Jagannadham, Thermal conductivity of copper-graphene composite films synthesized by electrochemical deposition with exfoliated graphene platelets, *Metallurgical and Materials Transactions B* 43 (2012) 316–324.
- [28] K. Jagannadham, Volume fraction of graphene platelets in copper-graphene composites, *Metallurgical and Materials Transactions A* 44 (2013) 552–559.
- [29] P. Goli, H. Ning, X. Li, C. Y. Lu, K. S. Novoselov, A. A. Balandin, Thermal properties of graphene–copper–graphene heterogeneous films, *Nano Letters* 14 (2014) 1497–1503.
- [30] K. Bui, H. M. Duong, A. Striolo, D. V. Papavassiliou, Effective heat transfer properties of graphene sheet nanocomposites and comparison to carbon nanotube nanocomposites, *The Journal of Physical Chemistry C* 115 (2011) 3872–3880.
- [31] S. K. Chien, Y. T. Yang, C. K. Chen, A molecular dynamics study of the mechanical properties of graphene nanoribbon–embedded gold composites, *Nanoscale* 3 (2011) 4307–4313.
- [32] T. Zhang, Q. Xue, S. Zhang, M. Dong, Theoretical approaches to graphene and graphene-based materials, *Nano Today* 7 (2012) 180–200.
- [33] T. Mura, *Micromechanics of defects in solids*, Martinus Nijhoff Publishers, Dordrecht, 1987.

- [34] S. Nemat-Nasser, M. Hori, *Micromechanics: Overall Properties of Heterogeneous Materials*, Elsevier, New York, 1999.
- [35] S. Torquato, *Random Heterogeneous Materials: microstructure and macroscopic properties*, Springer-Verlag, New York, 2002.
- [36] A. Öchsner, G. Murch (Eds.), *Heat Transfer in Multi-Phase Materials, Vol. 2 of Advanced Structured Materials*, Springer, New York, 2011.
- [37] H. J. Böhm, A short introduction to basic aspects of continuum micromechanics, Tech. rep., Institute of Lightweight Design and Structural Biomechanics (ILSB), Vienna University of Technology, Vienna, <http://www.ilsb.tuwien.ac.at/links/downloads/ilsbrep206.pdf> (2014).
- [38] C. Pichler, G. Metzler, C. Niederegger, R. Lackner, Thermo-mechanical optimization of porous building materials based on micromechanical concepts: Application to load-carrying insulation materials, *Composites Part B: Engineering* 43 (2012) 1015–1023.
- [39] M. Kurska, K. Kowalczyk-Gajewska, H. Petryk, Multi-objective optimization of thermo-mechanical properties of metal-ceramic composites, *Composites Part B: Engineering* 60 (2014) 586–596.
- [40] K. Jagannadham, Electrical conductivity of copper–graphene composite films synthesized by electrochemical deposition with exfoliated graphene platelets, *Journal of Vacuum Science and Technology B* 30 (2012) 03D109.
- [41] T. Mori, K. Tanaka, Average stress in matrix and average elastic energy of materials with misfitting inclusions, *Acta Metallurgica* 21 (1973) 571–574.
- [42] J. C. Halpin, J. L. Kardos, The Halpin-Tsai equations: a review, *Polymer Engineering Science* 16 (1976) 344–352.
- [43] C. Nan, R. Birringer, D. R. Clarke, H. Gleiter, Effective thermal conductivity of particulate composites with interfacial thermal resistance, *Journal of Applied Physics* 81 (1997) 6692–6699.
- [44] L. Hu, T. Desai, P. Keblinski, Thermal transport in graphene-based nanocomposite, *Journal of Applied Physics* 110 (2011) 033517.
- [45] K. M. F. Shahil, A. A. Balandin, Graphene–multilayer graphene nanocomposites as highly efficient thermal interface materials, *Nano Letters* 12 (2012) 861–867.
- [46] Y. Benveniste, A new approach to the application of Mori-Tanaka’s theory in composite materials, *Mechanics of Materials* 6 (1987) 147–157.
- [47] J. Y. Li, On micromechanics approximation for the effective thermoelastic moduli of multi-phase composite materials, *Mechanics of Materials* 31 (1999) 149–159.
- [48] J. D. Eshelby, The determination of the elastic field of an ellipsoidal inclusion, and related problems, *Proceedings of the Royal Society of London A* 241 (1957) 376–396.

- [49] R. Hill, Elastic properties of reinforced solids: some theoretical principles, *Journal of the Mechanics and Physics of Solids* 11 (1963) 357–372.
- [50] Y. Benveniste, G. J. Dvorak, T. Chen, On diagonal and elastic symmetry of the approximate effective stiffness tensor of heterogeneous media, *Journal of the Mechanics and Physics of Solids* 39 (1991) 927–946.
- [51] T. Chen, G. J. Dvorak, Y. Benveniste, Mori-Tanaka estimates of the overall elastic moduli of certain composite materials, *Journal of Applied Mechanics* 59 (1992) 539–546.
- [52] R. Hill, A self-consistent mechanics of composite materials, *Journal of the Mechanics and Physics of Solids* 13 (1965) 213–222.
- [53] C. L. Tucker, E. Liang, Stiffness predictions for unidirectional short-fiber composites: Review and evaluation, *Composites Science and Technology* 59 (1999) 655–671.
- [54] A. C. Gavazzi, D. C. Lagoudas, On the numerical evaluation of Eshelby’s tensor and its application to elastoplastic fibrous composites, *Computational Mechanics* 7 (1990) 13–19.
- [55] Y. P. Qiu, G. J. Weng, On the application of Mori-Tanaka’s theory involving transversely isotropic spheroidal inclusions, *International Journal of Engineering Science* 28 (1990) 1121–1137.
- [56] A. Sihvola, Metamaterials and depolarization factors, *Progress in Electromagnetics Research* 51 (2005) 65–82.
- [57] K. Kowalczyk-Gajewska, Bounds and self-consistent estimates of overall properties for random polycrystals described by linear constitutive laws, *Archives of Mechanics* 61 (2009) 475–503.
- [58] S. Torquato, Effective stiffness tensor of composite media – I. Exact series expansions, *Journal of the Mechanics and Physics of Solids* 45 (1997) 1421–1448.
- [59] A. A. Balandin, Thermal properties of graphene and nanostructured carbon materials, *Nature Materials* 10 (2011) 569–581.
- [60] H. M. Ledbetter, E. R. Naimon, Elastic properties of metals and alloys. II. Copper, *Journal of Physical and Chemical Reference Data* 3 (1974) 897–935.
- [61] D. R. Lide (Ed.), *CRC Handbook of Chemistry and Physics*, CRC Press, Boca Raton, FL, 2005, <http://www.hbcpnetbase.com>.
- [62] S. V. Shulepov, *Physics of carbon-graphite materials*, Metallurgiya, Moscow, 1972.
- [63] P. Delhaès (Ed.), *Graphite and Precursors*, *World of Carbon*, Vol. 1, Gordon and Breach Science Publishers, Amsterdam, 2001.

- [64] Properties and characteristics of graphite, Tech. rep., Entegris Inc., Billerica, USA, <http://www.entegris.com/resources/assets/6205-7329-0513.pdf> (2013).
- [65] D. G. Cahill, Thermal conductivity measurement from 30 to 750 K: the 3ω method, *Review of Scientific Instruments* 61 (1990) 802–808.